BIOCHEMISTRY
including biophysical chemistry & molecular biology

Article

pubs.acs.org/biochemistry

Kinetic Mechanism of Human Histidine Triad Nucleotide Binding Protein 1

Xin Zhou,[†] Tsui-Fen Chou,[†] Brandon E. Aubol,[§] Chin Ju Park,[‡] Richard Wolfenden,[∥] Joseph Adams,[§] and Carston R. Wagner*,[†]

[†]Department of Medicinal Chemistry and [‡]Minnesota NMR Facility, University of Minnesota, Minneapolis, Minnesota 55455, United States

[§]Department of Pharmacology, University of California—San Diego, La Jolla, California 92093, United States

[∥]Department of Biochemistry, University of North Carolina, Chapel Hill, North Carolina 27599, United States

Supporting Information

ABSTRACT: Human histidine triad nucleotide binding protein 1 (hHint1) is a member of a ubiquitous and ancient branch of the histidine triad protein superfamily. hHint1 is a homodimeric protein that catalyzes the hydrolysis of model substrates, phosphoramidate and acyl adenylate, with a high efficiency. Recently, catalytically inactive hHint1 has been identified as the cause of inherited peripheral neuropathy [Zimon, M., et al. (2012) *Nat. Genet. 44*, 1080−1083]. We have conducted the first detailed kinetic mechanistic studies of hHint1 and have found that the reaction mechanism is consistent with a double-displacement mechanism, in which the active site nucleophile His112 is first adenylylated by the substrate, followed by hydrolysis of the AMP−enzyme intermediate. A transient burst phase followed by a linear phase from the stopped-flow fluorescence assay indicated that enzyme adenylylation was faster than the subsequent intermediate hydrolysis and product release. Solvent viscosity experiments suggested that both chemical transformation and diffusion-sensitive events (product release or protein conformational change) limit the overall turnover. The catalytic trapping experiments and data simulation indicated that the true k_{off} rate of the final product AMP is unlikely to control the overall k_{cat}. Therefore, a protein conformational change associated with product release is likely rate-limiting. In addition, the rate of Hint1 adenylylation was found to be dependent on two residues with pK_a values of 6.5 and 8, with the former pK_a agreeing well with the nuclear magnetic resonance titration results for the pK_a of the active site nucleophile His112. In comparison to the uncatalyzed rates, hHint1 was shown to enhance acyl-AMP and AMP phosphoramidate hydrolysis by 10^6−10^8-fold. Taken together, our analysis indicates that hHint1 catalyzes the hydrolysis of phosphoramidate and acyl adenylate with high efficiency, through a mechanism that relies on rapid adenylylation of the active residue, His112, while being partially rate-limited by intermediate hydrolysis and product release associated with a conformational change. Given the high degree of sequence homology of Hint proteins across all kingdoms of life, it is likely that their kinetic and catalytic mechanisms will be similar to those elucidated for hHint1.

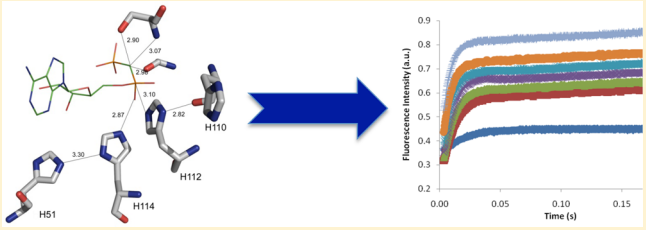

Histidine triad nucleotide binding proteins (Hints) are members of the histidine triad (HIT) protein superfamily of nucleotidyl transferases and hydrolases that contain a highly conserved active site motif of His-X-His-X-His-XX, where X is a hydrophobic amino acid[2] (Figure 1A). The Hint branch is the most ancient and is ubiquitously expressed in both prokaryotes and eukaryotes; however, their biological roles have not been fully characterized. Although initially Hint1 was reported as a protein kinase C inhibitor,[3] subsequent studies have not supported this observation.[4−6] Hint1 also was thought to be a zinc binding protein because of the presence of four histidines in the active site;[3] however, a rationale for this potentiality has not been forthcoming.

Recently, Hint1 has emerged as a tumor suppressor through multiple molecular mechanisms involving the regulation of apoptosis,[7] gene transcription,[8−11] and the cell cycle.[12,13] *Hint1*-deleted mice have an increased susceptibility to the carcinogenic DMBA (7,12-dimethylbenzanthracene)-induced ovarian and mammary tumors, as well as the increased frequency of spontaneous tumors.[14] Hint1 expression appears to correlate with the downregulation of p53 and the pro-apoptotic factor Bax.[7] Consistent with this finding and a potential role in tumorgenesis, Hint1 has been found to be associated with the Bax promoter and is a component of the Tip60 histone acetyltransferase complex.[15] Two hybrid screening experiments revealed that Hint1 was associated with cyclin-dependent kinase 7 (Cdk7); however, knockout mice studies failed to reveal a phenotype consistent with the regulation of Cdk7, indicating that Hint1 is not required for Cdk7 function.[16]

Received: December 2, 2012
Revised: March 8, 2013
Published: April 24, 2013

dx.doi.org/10.1021/bi301616c | *Biochemistry* 2013, 52, 3588−3600

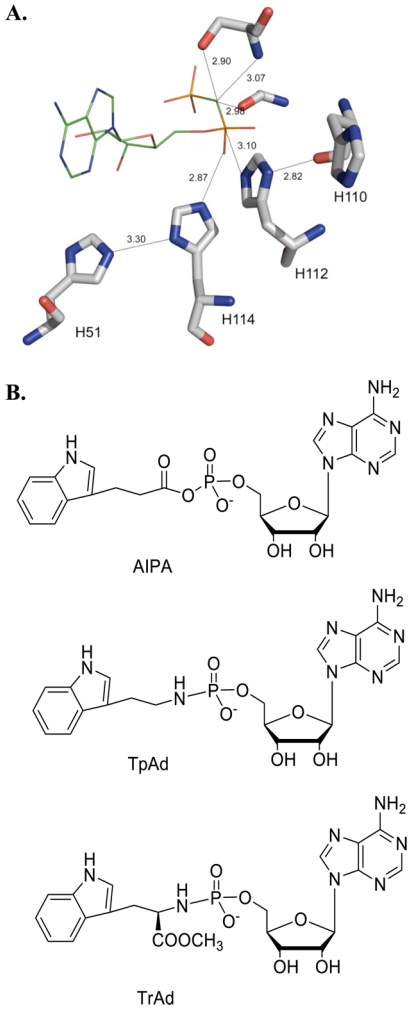

Figure 1. (A) Active site of hHint1 with AMP binding (PDB entry 1KPF). (B) Structures of substrates.

Evidence has also accumulated that eukaryotic Hint1 is associated with several gene transcription factors, such as TFIIH,[8] MITF,[9,10] and USF2.[11] In addition to their emerging role in cancer, a link between Hint1 and the regulation of postsynaptic dopamine transmission[17,18] and the development of hepatic ischemia reperfusion injury has been discovered.[19]

While a variety of interactions with Hint1 have been discovered, little is known about the enzymatic activity and the underlying catalytic mechanism, as well as the possible linkage between enzymatic activity and intracellular function(s). It has been suggested that Hint enzymatic activity is inhibited via heterodimerization with Asw (avian sex-specific W-linked) protein, a potentially sex-determining protein in birds.[20,21] Brenner and co-workers have reported that rabbit Hint1 and yeast HNT hydrolyze adenosine 5′-monophosphoramidate (AMP-NH_2) to AMP and ammonia, and adenosine lysine phosphoramidate to AMP and lysine,[22] while Wagner and co-workers demonstrated by ^{31}P nuclear magnetic resonance (NMR) that human Hint1 and *Escherichia coli* HinT (ycfF) are efficient purine nucleoside phosphoramidases.[23−25] Substrate specificity studies have revealed a preference of Hint1s for nucleoside phosphoramidate substrates containing purine ribonucleosides coupled to unhindered alkyl amine.[24] In addition, acyl nucleoside monophosphates were found to be modestly better substrates for both ecHinT and hHint1, with k_{cat}/K_m values ranging from 10^6 to 10^8 M^{-1} s^{-1}. Because acyl-AMP generated by lysyl t-RNA synthetase has also been shown to be a good substrate of both bacterial and human Hint1, Chou and co-workers have proposed that acyl-AMP prepared by AARSs may be the natural substrate of Hints.[26] Intriguingly, Wang and co-workers recently have determined the crystal structures of Hint1 in complex with aminoacyl adenylate analogues and revealed that Hint1 broadly recognizes only the common main chain of the aminoacyl moiety, without specifically interacting with the amino acid side chain.[27] Although Hints are unable to conduct phosphate hydrolysis, Krakowiak and co-workers have observed that Hint1 is capable of cleaving the P−S bond of nucleoside 5′-*O*-phosphorothiolates, suggesting that the production of H_2S during the desulfuration reaction catalyzed by Hint1 may be biologically significant.[28]

While efficient phosphoramidases and acyl-AMP hydrolases have been described, until recently a direct connection between Hint1 catalysis and a biological phenotype has proven to be elusive. Yeast genetic and growth studies by Breiganowski and co-workers established that the growth of yeast on galactose is dependent on Hnt activity,[29] while Chou and co-workers demonstrated that Hint activity is necessary for the growth of *E. coli* under high-salt conditions.[23] Bardaweel and co-workers have further demonstrated that the activity of *E. coli* D-alanine dehydrogenase, and therefore growth on alanine, is dependent on *E. coli* Hint (ecHinT) catalysis.[30] Recently, hHint loss of function has been proposed as a cause of inherited peripheral neuropathy, a condition that affects 1 in 2500 individuals.[1] A genomewide SNP analysis of 33 families exhibiting inherited peripheral neuropathy found a strong correlation between the loss of catalytically functional hHint1 and autosomally recessive axonal neurophathy with neuromyotonia, thus providing evidence for the first phenotype linked to hHint1 enzymatic activity.[1]

Although the HIT superfamily is comprised of five and possibly six distinct subfamilies, investigations of their catalytic and kinetic mechanisms of action have been conducted with only GalT and Fhit. In both cases, catalysis proceeds by formation of a histidine-NMP intermediate with inversion of the phosphorus configuration, followed by transfer to either water (Fhit) or galactose (GalT). For GalT, uridylylation of the nucleophilic histidine by UDP-glucose and the subsequent deuridylylation by galactose 1-phosphate were found to be rapid with rates of 281 and 166 s^{-1} at 4 °C, respectively.[31] Because these two rates were higher than the k_{cat} value (62 s^{-1} at 4 °C), it has been proposed that either product release or a conformational change may be rate-limiting.[31] Most importantly, structural analysis of the GalT active site revealed that two of the conserved histidines and a proximal cysteine formed a coordinate complex with an atom of Fe.[32] For Fhit, while conversion of Ap_3A to ADP and AMP proceeds through a double-displacement mechanism, less is known about the specific catalytic steps.[33] When the putative nucleophilic histidine was replaced with glycine, free imidazole was found to rescue enzymatic activity.[34] In addition, AMP-imidazole and AMP-*N*-methylimidazole were found to be substrates.[35] Results of steady-state kinetic and mutagenesis studies have implied that one member of the catalytic triad, His98, is likely responsible for the donation of a proton to the leaving group, as well as substrate binding.[34] This is in marked contrast to GalT, in which the corresponding histidines are coordinated to Fe. Because there is no evidence of significant coordination of

dx.doi.org/10.1021/bi301616c | *Biochemistry* 2013, 52, 3588−3600

Fe or metal to the active site histidines of either Fhit or Hints, Hint1 appears to be catalytically similar to Fhit, and not GalT. Nevertheless, a detailed kinetic mechanism for either enzyme has yet to be elucidated.

The catalytic mechanism of Hint1 has been proposed to proceed through a two-step double-displacement mechanism, analogous to that of Fhit, in which His112 is thought to form a covalent Hint-AMP intermediate followed by hydrolysis and the release of AMP[26,36] (Figure 1A). However, a detailed picture of the catalytic and kinetic mechanism of Hint1 has yet to be elucidated. Phosphoramidates, such as TpAd and TrAd, and amino acyl mimics such as AIPA (Figure 1B) can undergo P−N bond and P−O bond cleavage by Hint1, respectively. Because of the ability of nucleosides to quench the fluorescence of the covalently linked indole moiety of tryptamine (Figure 1B), we have developed a sensitive continuous fluorescence assay using these model substrates, TpAd and AIPA.[24,37]With these tools, we have been able to delineate the kinetic mechanism and features of the catalytic mechanism of Hint1 by site-directed mutagenesis, pre-steady-state and steady-state kinetic analyses, solvent viscometric studies, and kinetic model fittings. The results of these studies shed light on the parameters influencing Hint1 catalysis in particular and the HIT superfamily in general.

MATERIALS AND METHODS

Materials. AMP, AMP-agarose, ampicillin, chloramphenicol, HEPES, $MgCl_2$, and sucrose were purchased from Sigma-Aldrich (St. Louis, MO). TpAd and AIPA were synthesized following the procedures published in refs 24 and 37, respectively. Steady-state kinetic data were collected on a Varian (Palo Alto, CA) Cary Eclipse fluorimeter with the kinetic program equipped with a thermostated cuvette holder. Transient kinetic data were obtained on a single-wavelength stopped-flow apparatus (model SX.18MV, Applied Photophysics, Leatherhead, U.K.). Kinetic data were analyzed with JMP IN version 7 (SAS Institute, Inc., Cary, NC).

Site-Directed Mutagenesis, Protein Expression, and Purification. The active site mutations, H51A, H110A, H112G, and H114A, were generated using the human Hint1-pSGA02 vector with QuickChange site-directed mutagenesis kit (Stratagene, La Jolla, CA). The oligonucleotide primers were 5′-CAA GCA CCA ACA GCT TTT CTG GTG ATA CC-3′, 5′-CAG TCT GTC TAT GCC GTT CAT CTC CAT G-3′, 5′-GTC TAT CAC GTT GCT CTC CAT GTT CTT GG-3′, and 5′-CAC GTT CAT CTC GCT GTT CTT GGA GG-3′, respectively. The wild-type and mutated human Hint1-pSGA02 plasmids were transformed into *E. coli* hinT disrupt ted strain BB2 as previously described.[23] The expression and purification of the mutants were similar to those for the wild type, which followed a previously published procedure.[23] Briefly, an AMP-agarose column was applied after the cell lysis by lysozyme and sonication. Hint protein was eluted with a 25 mM AMP solution. A PD-10 column was employed to desalt the protein samples. Protein concentrations were determined with the Bradford protein assay.[38]

Stopped-Flow Fluorescence Analysis of Adenylylation of Human Hint1. As mentioned above, we have developed a continuous and sensitive fluorescence assay using two fluorogenic substrates, TpAd and AIPA. Because of the magnitude of fluorescence quenching (>20-fold), hydrolysis of TpAd or AIPA by Hint1 leads to an increase in the indole fluorescence from tryptamine, the product for the first half-reaction. This fluorescence increase can be monitored with time in stopped-flow kinetic experiments and can be used to measure the reaction rates of the adenylylation of human Hint1 as well, if the hydrolysis of adenylylated Hint1 is much slower than formation of the adenylylated Hint1 intermediate. Therefore, we monitored the reaction rates of the adenylylation of Hint1 at 25 °C using a fluorescence stopped-flow apparatus (Applied Photophysics, model SX.18MV). AIPA (5−40 μM) or TpAd (5−60 μM) in HEPES buffer [20 mM HEPES and 1 mM $MgCl_2$ (pH 7.2)] was transferred to one stopped-flow syringe, and human Hint1 (WT, 69 μg/mL, 5 μM) in HEPES buffer [20 mM HEPES and 1 mM $MgCl_2$ (pH 7.2)] was transferred to the other syringe. Each time, equal volumes (50 μL) of the enzyme solution and the substrate were injected and mixed rapidly. The excitation wavelength was set to 280 nm, and the fluorescence was monitored through a 320 nm cutoff filter. The time course curves (burst kinetics) were fit by a single-exponential equation with a steady-state term (eq 1) using JMP IN version 7

$$P(t) = Ae^{-k_b t} + k_l t + C \quad (1)$$

where A is the amplitude of the burst, k_l is the linear rate of increase of fluorescence, and k_b is the burst rate, or the observed pseudo-first-order rate constant. The results represent the average of six experiments. The kinetic parameters, k_2, $K^{adenylyl}$, and $k_2/K^{adenylyl}$, for AIPA or TpAd reaction were obtained by nonlinear fitting of the data to eqs 1 and 2

$$k_b = \frac{k_2[S]}{K^{adenylyl} + [S]} \quad (2)$$

where [S] is the substrate concentration.

Active Site Titration. In the active site titration experiment, human Hint1 (1, 2, 3, 4, or 5 μM) in HEPES buffer was mixed with AIPA (10 μM) and the fluorescence intensity was monitored. The time course data were fit to eq 1. The amplitude, A, which represents a measure of the number of moles of adenylylated enzyme in the first catalytic cycle, can be plotted linearly versus the Hint1 monomer concentration, and the slope indicates the active site percentage per monomer.

Steady-State Fluorescence Assay of Human Hint1. The steady-state fluorescence assay was performed at 25 °C using a Varian/Cary Eclipse fluorimeter as described previously.[24] For the standard assay, the hydrolysis of the fluorogenic substrate by human Hint1 was conducted in degassed HEPES buffer [20 mM HEPES and 1 mM $MgCl_2$ (pH 7.2)] in quartz cuvettes. The excitation wavelength was set to 280 nm, and the emission fluorescence was measured at 360 nm. The excitation and emission slits were set at 5 nm. The initial velocity of hydrolysis was measured with hH1 or mutant (6−50 nM) and varied concentrations of either phosphoramidate (0−10 μM) or acyl adenylate (0−10 μM). The curves were fit to eq 3 to yield the first-order rate constant, k_{cat}, and the apparent Michaelis−Menten constant, K_m, using JMP IN version 7

$$v = \frac{k_{cat}[E]_t[S]}{K_m + [S]} \quad (3)$$

where v is the initial velocity, $[E]_t$ is the total enzyme concentration, and [S] is the substrate concentration.

Solvent Viscosity Effect Experiments. The viscosity of the solution was controlled by the addition of appropriate amounts of microviscosogen, sucrose, or macroviscosogen,

Scheme 1. Proposed Minimal Four-Step Mechanism of hHint1

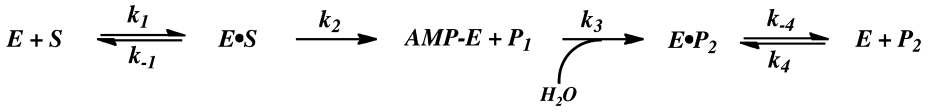

PEG8000. The relative viscosities (η^{rel}) of the solution were taken from ref 39. The steady-state first-order rate constants (k_{cat}) and apparent Michaelis–Menten constants (K_m) were determined as described above in HEPES buffer [20 mM HEPES and 1 mM $MgCl_2$ (pH 7.2)] containing the appropriate amounts of sucrose (0, 14, 24, or 32%) or PEG8000 (5%). A minimal four-step mechanism that includes a kinetically significant product release is shown in Scheme 1, in which the observed k_{cat} is a combination of two chemistry steps (adenylylation and hydrolysis) and one diffusive step (eq 6).

$$K_{adenylyl} = \frac{k_{-1} + k^2}{k_1} \quad (4)$$

$$k_2/K_{adenylyl} = \frac{k_1 k_2}{k_{-1} + k_2} \quad (5)$$

$$k_{cat} = \frac{1}{\frac{1}{k_2} + \frac{1}{k_3} + \frac{1}{k_{-4}}} \quad (6)$$

$$K_m = \frac{1 + \frac{k_{-1}}{k_2}}{k_1\left(\frac{1}{k_2} + \frac{1}{k_3} + \frac{1}{k_{-4}}\right)} \quad (7)$$

$$\frac{k_{cat}}{K_m} = \frac{k_1}{1 + \frac{k_{-1}}{k_2}} \quad (8)$$

Data were fit using eqs 9–11.

$$\frac{(k_{cat}/K_m)^0}{k_{cat}/K_m} = \frac{k_1}{k_2 + k_{-1}} \times \eta^{rel} + \frac{k_{-1}}{k_2 + k_{-1}} \quad (9)$$

$$\frac{k_{cat}^{\ 0}}{k_{cat}} = \frac{\frac{1}{k_{-4}}}{\frac{1}{k_2} + \frac{1}{k_3} + \frac{1}{k_{-4}}} \times \eta^{rel} + \frac{\frac{1}{k_2} + \frac{1}{k_3}}{\frac{1}{k_2} + \frac{1}{k_3} + \frac{1}{k_{-4}}} \quad (10)$$

$$\frac{1}{k_{cat}} = \frac{1}{k_{-4}} \times \eta^{rel} + \frac{k_2 + k_3}{k_2 k_3} \quad (11)$$

where $k_{cat}^{\ 0}$ and $(k_{cat}/K_m)^0$ represent the kinetic parameters in the absence of microviscosogen and k_{cat} and k_{cat}/K_m those in its presence.

pH Dependence of Pre-Steady-State Parameters. At pH values ranging from 5.8 to 9.0, the adenylylation kinetic parameters for the first half-reaction, k_2 and $k_2/K^{adenylyl}$, were determined using stopped-flow apparatus with human Hint1 (final WT concentration of 2.5 μM) and TpAd (5–60 μM) or AIPA (2.5–20 μM) in phosphate buffer (100 mM). Assays were performed as described for the pre-steady-state kinetic experiments (*vide supra*). The time course curves were first fit with eq 1 to obtain the values for k_b, and then k_2 and $k_2/K^{adenylyl}$ were obtained for each pH from the fitting with eq 2. To fit the k_2 versus pH data for the WT, eq 12 was used (Scheme 2).

pH Dependence of Steady-State Kinetic Parameters. The pH–rate profiles of steady-state hydrolysis of phosphoramidate by Hint1 and mutants were determined with a

Scheme 2

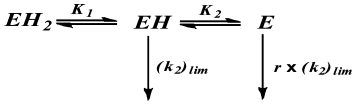

$$(k_2)_{obs} = \frac{(k_2)_{lim}}{\frac{[H^+]}{K_1} + 1 + \frac{K_2}{[H^+]}} + \frac{r \times (k_2)_{lim}}{1 + \frac{[H^+]^2}{K_1 K_2} + \frac{[H^+]}{K_2}}$$

$$Log(k_2)_{obs} = \log\left(\frac{(k_2)_{lim}(1 + r \times 10^{(pKa_2^{adenylyl} - pH)})}{10^{(pH - pKa_1^{adenylyl})} + 1 + 10^{(pKa_2^{adenylyl} - pH)}}\right) \quad (12)$$

saturating substrate concentration (50 μM) and an appropriate enzyme concentration (0.0625–0.25 μM) in phosphate buffer (100 mM, pH 5.8–9). The k_{cat} versus pH data were fit with eq 13.

Determination of Dissociation Constants (K_d) by Tryptophan Fluorescence Titration. Titration with AMP was performed using hHint1 (6 μM) in 1.5 mL of HEPES buffer [20 mM HEPES and $MgCl_2$ (pH 7.2)]. The AMP stock was added, and the mixture was stirred for 30 s; then the emission fluorescence intensity ranging from 300 to 450 nm was measured for 30 s at a scan speed of 300 nm/min (excitation at 280 nm). The peak fluorescence intensity at ~351 nm was obtained from the average intensities of 349–353 nm. Appropriate corrections were made for dilution effects (never exceeding 10%). Data were fit to eq 14for fluorescence titration of ligand binding:

$$F = F_e - \left\{[[E]_t + [L]_t + K_d - \sqrt{([E]_t + [L]_t + K_d)^2 - 4[E]_t[L]_t}](F_e - F_{el})\right\} / (2[E]_t) \quad (14)$$

where F is the fluorescence intensity, F_e is the fluorescence intensity of the protein without ligand binding, F_{el} is fluorescence intensity of the protein with ligand binding, $[E]_t$ is the total concentration of the protein, $[L]_t$ is the total concentration of the ligand, and K_d is the dissociation constant.

Catalytic Trapping Experiments. WT human Hint1 (5 μM) was preincubated with AMP (0–5000 μM) in one stopped-flow syringe for 10 min and then mixed with TpAd (40 μM) in the other syringe. The time course of the reaction was monitored as previously described. To minimize the inner filter effect, the concentration of AMP was controlled not to exceed 5% of the absorbance.

NMR Spectroscopy Analysis of Histidine pK_a Changes in Human Hint1. WT hHint1 and H112A were purified by an AMP-agarose column from echinT deletion stain (BB2) as described previously.[23] Purified protein was exchanged with phosphate buffer in H_2O at different pH values [0.1 M sodium phosphate (pH 6.00–9.00)] and concentrated to 8 mg/mL; 300 μL of a protein sample was transferred to a new tube, frozen, and lyophilized. After lyophilization, the samples were reconstituted in 300 μL of 99.8% D_2O. Further proton exchange was conducted by storing the samples at 4 °C for

dx.doi.org/10.1021/bi301616c | *Biochemistry* 2013, 52, 3588–3600

Table 1. Pre-Steady-State Kinetics of hHint1 Using AIPA or TpAd as the Substrate in HEPES Buffer [20 mM HEPES and 1 mM $MgCl_2$ (pH 7.2)] at 25 °C

	AIPA			TpAd		
	k_2 (s^{-1})	$K^{adenylyl}$ (μM)	$k_2/K^{adenylyl}$ (M^{-1} s^{-1})	k_2 (s^{-1})	$K^{adenylyl}$ (μM)	$k_2/K^{adenylyl}$ (M^{-1} s^{-1})
WT	443 ± 38	5 ± 1	(8.8 ± 2.8) × 10^7	203 ± 13	13 ± 2	(1.6 ± 0.4) × 10^7
H114A	851 ± 45	35 ± 5	(2.4 ± 0.5) × 10^7	34 ± 1	57 ± 7	(0.6 ± 0.1) × 10^6
H110A	965 ± 83	15 ± 4	(6.4 ± 2.0) × 10^7	29 ± 1	12 ± 2	(2.5 ± 0.4) × 10^6
H51A	313 ± 12	17 ± 2	(1.8 ± 0.3) × 10^7	23 ± 1	27 ± 2	(0.9 ± 0.1) × 10^6

Table 2. Steady-State Kinetics of hHint1 in HEPES Buffer [20 mM HEPES and $MgCl_2$ (pH 7.2)] at 25 °C

	AIPA				TpAd			
	k_{cat} (s^{-1})	k_l[a] (s^{-1})	K_m (μM)	k_{cat}/K_m (M^{-1} s^{-1})	k_{cat} (s^{-1})	k_l[a] (s^{-1})	K_m (μM)	k_{cat}/K_m (M^{-1} s^{-1})
WT	1.98 ± 0.02	2.7 ± 0.8	0.04 ± 0.002	(5.3 ± 0.5) × 10^7	2.1 ± 0.1	2.0 ± 0.4	0.13 ± 0.02	(1.5 ± 0.3) × 10^7
H114A	0.69 ± 0.05	0.23 ± 0.05	0.12 ± 0.01	(0.6 ± 0.1) × 10^7	0.29 ± 0.02	0.14 ± 0.01	0.27 ± 0.05	(1.1 ± 0.3) × 10^7
H110A	0.60 ± 0.02	0.16 ± 0.02	0.04 ± 0.004	(1.6 ± 0.2) × 10^7	0.24 ± 0.01	0.18 ± 0.02	0.08 ± 0.01	(2.9 ± 0.4) × 10^6
H51A	0.98 ± 0.06	0.33 ± 0.04	0.05 ± 0.03	(1.9 ± 0.2) × 10^7	0.53 ± 0.02	0.27 ± 0.03	1.8 ± 0.2	(0.3 ± 0.04) × 10^6

[a] k_l represents the linear rate calculated from pre-steady-state measurements.

40 h. Before NMR analysis, the samples were centrifuged at 13000*g* for 10 min, and the supernatant was transferred to a Shigemi 5 mm NMR microtube assembly (matched with D_2O, bottom length of 15 mm, type BMS-3 from Shigemi Inc., Allison Park, PA). The one-dimensional (1D) proton NMR and TOCSY spectra were acquired on 600 MHz Varian Inova 6001 spectrometers equipped with a Bioselect probe at 25 °C. Histidine C-2 proton resonances were well-resolved and assigned by comparison of spectra under the continuous closely spaced pH values. The pK_a values were obtained by nonlinear fitting of the titration data to the modified Henderson–Hasselbalch equation (eq 15)[40]

$$\delta_{obs} = \delta_{obs} + (\delta_{H^+} - \delta_H) \times 10^{-pK_a}/(10^{-pK_a} + 10^{-pH}) \quad (15)$$

where δ_{obs}, δ_{H+}, and δ_H are the chemical shifts for the observed, protonated, and neutral imidazoles, respectively.

Determination of the Uncatalyzed Rate of TpAd and AIPA Hydrolysis. The uncatalyzed rates of hydrolysis of TpAd and AIPA were determined by monitoring the reaction in a quartz sealed tube as previously described with minor modifications.[41] Reaction mixtures containing the anhydride AIPA (0.05 M) in aqueous potassium phosphate buffer (0.1 M, pH 6.8) were incubated at temperatures from 10 to 47 °C for various amounts of time. Reactions were then stopped when the mixtures were frozen, and the product mixtures were analyzed by proton NMR (500 MHz) after 10-fold dilution with D_2O solutions containing added pyrazine (0.01 M, δ 8.60 ppm) as an integration standard. Hydrolysis of the anhydride linkage of AIPA was accompanied by the disappearance of a doublet at 5.88 ppm and the appearance of a doublet associated with the product AMP at 6.08 ppm (confirmed by addition of the authentic molecule), and also by the disappearance of a doublet at 7.35 ppm and the appearance of a doublet at 7.45 ppm associated with the product indolepropionic acid (confirmed by addition of the authentic molecule). Reaction mixtures containing TpAd (0.05 M) in aqueous potassium phosphate buffer (0.1 M, pH 6.8) were incubated at temperatures ranging from 59 to 121 °C for various amounts of time. Reactions were then stopped when the mixtures were cooled, and the product mixtures were analyzed by proton NMR (500 MHz) after 10-fold dilution with D_2O solutions containing added pyrazine (0.01 M, δ 8.60 ppm) as an integration standard. Hydrolysis of the phosphoramide linkage of TpAd was accompanied by the disappearance of a doublet at 5.90 ppm and the appearance of a doublet associated with the product AMP at 6.08 ppm (confirmed by addition of the authentic molecule).

RESULTS

Transient-State Kinetics. We have observed that the hydrolysis of TpAd or AIPA results in a significant increase in the fluorescence intensity, because of the release of tryptamine, allowing us to monitor spectrophotometrically the steady-state and transient-state kinetics of the reaction.[42,43] Stopped-flow fluorescence of human Hint1 using the phosphoramidate substrate, TpAd, or acyl adenylate substrate, AIPA, displayed an initial "burst" phase followed by a linear steady-state phase (Figure S1A of the Supporting Information). The burst phase suggested rapid formation of an intermediate within the first catalytic cycle, while the linear steady-state phase (k_l) suggested a slow rate-limiting step following intermediate formation. Data fitting analysis revealed k_l values of 2.0 ± 0.4 and 2.7 ± 0.8 s^{-1} for TpAd and AIPA, respectively (Table 1). These values agreed well with the observed steady-state k_{cat} values of 2.1 ± 0.1 and 1.98 ± 0.02 s^{-1} for TpAd and AIPA (Table 2), respectively, thus suggesting that intermediate hydrolysis and/or product release steps are likely rate-limiting.

Because of a single tryptophan (Trp123) in the C-terminus, hHint1 exhibits fluorescence (excitation at 280 nm, emission at 340 nm). To rule out the possibility that the observed fluorescence burst might originate from a change in hHint1 fluorescence, we prepared the Trp123 to Ala mutant, demonstrated that the protein fluorescence had been abolished, and then examined the hydrolysis of AIPA by W123A with stopped-flow kinetics. Compared to those of WT hHint1 (k_2 = 443 s^{-1}; $K^{adenylyl}$ = 5 μM), the W123A mutant exhibited a similar burst rate and a slightly increased $K^{adenylyl}$ (k_2 = 301 s^{-1}; $K^{adenylyl}$ = 8 μM). The reduced rate for the burst also agrees with the previous notion that W123 affects Hint enzymatic activity. Furthermore, fluorescence quenching, presumably from the enzyme, was observed when the catalytically inactive mutant, H112A, was mixed with substrate, which is consistent with the observed fluorescence increase during the reaction arising from substrate hydrolysis.

dx.doi.org/10.1021/bi301616c | *Biochemistry* 2013, 52, 3588–3600

Next, we characterized the burst kinetics for TpAd and AIPA. As one can see in panels B and C of Figure S1 of the Supporting Information, the burst rate was found to be hyperbolic and substrate concentration-dependent for both TpAd and AIPA. The upper limits of the burst rate (k_b) suggest that the adenylylation rates (k_2) of Hint1 for AIPA and TpAd are 443 and 203 s^{-1}, respectively (Table 1). Notably, the second-order rate constants, $k_2/K^{adenylyl}$, for AIPA and TpAd are $(8.8 \pm 2.8) \times 10^7$ and $(1.6 \pm 0.4) \times 10^7$ M^{-1} s^{-1}, respectively, which approach the diffusion limit (10^8–10^{10} M^{-1} s^{-1}). Thus, the efficiency of the enzyme during the first step (adenylylation) is quite high, and the substrate is likely to be "sticky" ($k_{-1} \ll k_2$), limiting dissociation of the substrate from the enzyme prior to intermediate formation. With sticky substrates, the slopes of the linear portion at low substrate concentrations approached the association rate constants (k_1)[44] for AIPA and TpAd of 6×10^7 and 1×10^7 M^{-1} s^{-1}, respectively. The correspondence of these values of k_1 with the steady-state k_{cat}/K_m values (eq 8) supports this assertion.

To assess the degree of cooperativity between the two active sites of hHint1, we examined the burst amplitude, because it is indicative of the number of product molecules turned over in the first catalytic cycle and thus the active enzyme concentration. As one can see in Figure 2B, the burst amplitude was found to be dependent on enzyme concentration.

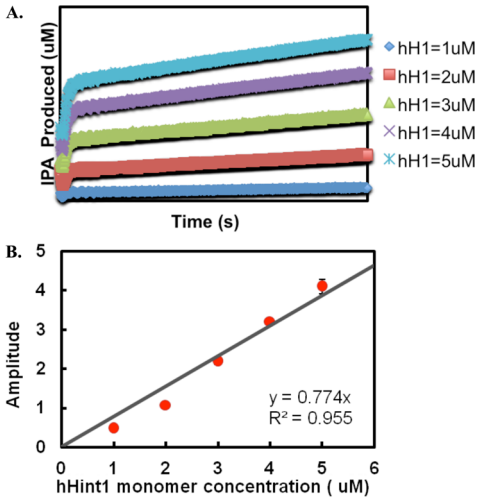

Figure 2. Active site titration. (A) WT human Hint1 (1, 2, 3, 4, and 5 μM) was mixed with AIPA (10 μM) in a stopped-flow cell, and the time course of IPA production was monitored at 360 nm. (B) Amplitude of the burst vs human Hint1 monomer concentration. A slope of 0.77 with an R^2 of 0.955 indicated that 77% of the active site catalyzes the reaction in the first catalytic cycle.

Plotting the amplitude versus the hHint1 monomer concentration yielded a linear correlation with a slope of 0.77 [R^2 = 0.955 (Figure 2B)], indicating employment of 77% of the active sites in the first catalytic cycle. Thus, the amplitude of the burst is stoichiometric with the calculated Hint monomer concentration, indicating little cooperativity between the two active sites.

Inspection of the active site of hHint1 has revealed that in addition to the active site nucleophile (His112), His51, His110, and His114 are also strictly conserved (Figure 1A). Although it is not close enough to hydrogen bond to His112, His114 has been shown to be in the proximity of the phosphate oxygens of bound AMP. His51 appears to form a close hydrogen bond to His114, while the backbone carbonyl of His110 forms a hydrogen bond to His112. We addressed the role of each of these residues in the burst phase of the reaction with AIPA and TpAd by site-directed mutagenesis. Regardless of the mutant or the substrate, a rapid burst phase was observed. For AIPA, the value of the burst phase increased approximately 2-fold, from 443 s^{-1} for the WT to 851 and 965 s^{-1} for mutants His114Ala and His110Ala, respectively. In contrast, each of the mutants reduced the burst phase rate when TpAd was the substrate from 203 to 23–34 s^{-1}. This discrepancy suggests that somewhat different catalytic mechanisms may be employed for hydrolysis of TpAd and AIPA by these mutants. As a potential proton donor, H114 could possibly transfer a proton to the phosphoryl oxygen, which is 2.87 Å away, which could be transferred to the amine of the amino group facilitating TpAd P–N bond cleavage. In contrast, dissociation of the acyl product generated by the AIPA reaction may be accelerated in the absence of H114 and proton transfer, assuming charge repulsion is a sufficient driving force. Because stabilization of H114 by H51 may promote the proton transfer, it is possible that in the absence of H51, hydrolysis of TpAd is more affected than AIPA hydrolysis. Because crystal structure analysis demonstrates that the backbone carbonyl of His110 hydrogen bonds to the imidazole of H112, but not H114, H110 is likely to stabilize deprotonated H112, which would be required for both TpAd and AIPA hydrolysis. The similar impact of the H110A mutant on the rate of adenylation by both substrates supports this assertion.

The observed linear steady-state phase (k_l) observed for each of the mutants when AIPA is the substrate was reduced from 6.4- to 13-fold, while for TpAd, the rate was reduced from 7.3- to 14-fold (Table 2). Similar to those of the WT, the values of the linear rate are in agreement with the observed k_{cat} values for the mutants and each of the substrates (Table 2).

Examination of the $k_2/K^{adenylyl}$ values for AIPA revealed that while the k_2 value either increased for the His110Ala and His114Ala mutants or slightly decreased for the His51Ala mutant, the overall efficiencies of the mutants declined relative to that of the WT because of the increase in $K^{adenylyl}$. With the exception of the His110Ala mutant, the $K^{adenylyl}$ values for the mutant hHints increased with the TpAd substrate. Consequently, comparable lower values of k_2 resulted in significantly lower $k_2/K^{adenylyl}$ values for each of the active site mutants with TpAd.

Steady-State Kinetic Parameters. The Michaelis–Menten parameters for hHint1 with the substrates AIPA and TpAd were found to be nearly identical, resulting in similar k_{cat}/K_m values (Table 2), suggesting that the enzyme proceeds through similar rate-limiting steps for each substrate. Because the concentration of the second substrate (water) for a double-displacement mechanism (ping-pong mechanism) can be regarded as fixed and saturated, the steady-state k_{cat}/K_m approximates the pre-steady-state $k_2/K^{adenylyl}$. Indeed, the measured values of k_{cat}/K_m and $k_2/K^{adenylyl}$ are within a similar range. Each of the active site histidine mutations was found to lower the k_{cat} by 2–2.9-fold for AIPA and similarly 2.8–8.8-fold for TpAd. With the exception of the H51A mutant K_m for TpAd, which was 13.8-fold greater than the wild-type K_m, the K_m values for the mutants were either identical or within 3-fold of the value for WT hHint1.

Viscosity Effect Studies. Previous kinetic studies of Hints with phosphoramidate substrates have proposed that hydrolysis

dx.doi.org/10.1021/bi301616c | *Biochemistry* 2013, 52, 3588–3600

of the active site histidine adenylate is likely the rate-determining step.[24] Nevertheless, it is quite possible that product release may also be at least partially rate-limiting. Because the molecular diffusion rates vary inversely with the viscosity of the solvent, a diffusion-controlled rate-limiting step can be probed by a viscosity variation assay. With an increase in the viscosity of the solution with a microviscosogen such as sucrose, the rate of diffusion is lowered whereas the unimolecular reaction rate remains unperturbed. Thus, the diffusion-controlled steps in enzymatic pathways can be isolated, and the extent to which the diffusion-controlled steps limit the reaction rate can be estimated.

The rate of steady-state hydrolysis of TpAd by WT Hint1 was measured in the presence and absence of a micro-viscosogen, sucrose, in HEPES buffer at pH 7.2. From the kinetic mechanism proposed in Scheme 1, an increasing solvent microviscosity would be predicted to affect k_1, k_{-1}, k_4, and k_{-4}, but not k_2 or k_3, with the overall k_{cat} being dependent on a combination of k_2, k_3, and k_{-4} (eq 6).

According to eq 9, a linear plot of the ratio of the second-order rate constant without a viscosogen to the second-order rate constant with a viscosogen, $(k_{cat}/K_m)^0/(k_{cat}/K_m)$, versus relative viscosity, η^{rel}, yields the partition ratio for the ES complex, k_{-1}/k_2, as the reciprocal of the $k_2/(k_{-1} + k_2)$ slope subtracting unity. For a slope close to 1 (=0.9) (Figure 3A), $k_{-1} < k_2$ ($k_{-1}/k_2 = 0.1$), indicating that the first irreversible step along the reaction pathway is considerably faster than substrate dissociation. Thus, in agreement with the transient-state kinetics, the $k_2/K^{adenylyl}$ value for TpAd with hHint1 is near the diffusion-controlled limit (*vide supra*). In contrast, the relative first-order rate constant, k_{cat}^0/k_{cat}, was only 60% dependent on the solvent viscosity (Figure 3B, slope of 0.61). Thus, employing the expression for k_{cat}^0/k_{cat} (eq 10), the overall reaction rate was found to be nearly equally limited by an internal presumably chemistry (k_3) step and a diffusion-dependent (k_{-4}) step.

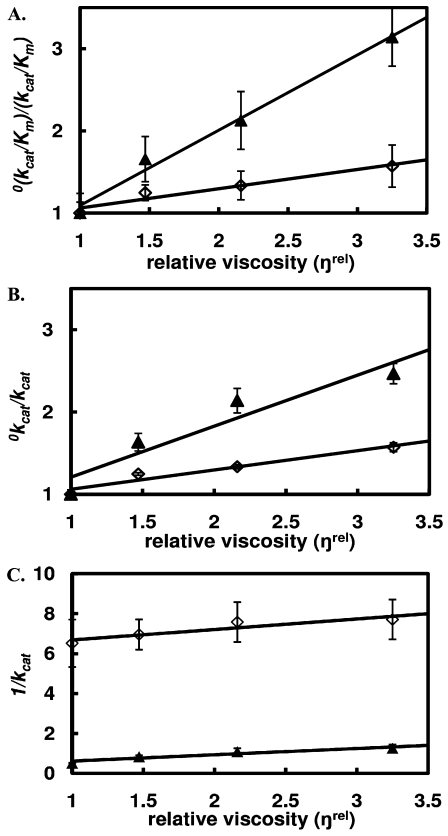

Figure 3. Effects of solvent viscosity on the steady-state hydrolysis of TpAd (▲) and TrAd (◇) in HEPES buffer at pH 7.2. (A) Plot of the relative second-order rate constant as a function of relative viscosity (η^{rel}). (B) Plot of the relative k_{cat} vs relative viscosity (η^{rel}). (C) Plot of $1/k_{cat}$ vs relative viscosity (η^{rel}).

When a plot of $1/k_{cat}$ versus relative viscosity, η^{rel}, was examined, a slope of 0.31 and an intercept of 0.30 were observed (Figure 3C). Employing eq 11 and a k_2 value of 203 s^{-1} determined from pre-steady-state studies (*vide supra*), a value of 3.33 s^{-1} could be calculated for k_{-4} and a value of 3.48 s^{-1} for k_3, thus indicating that the steady-state rate of hHint1 is partially rate-limited by an internal presumably chemical step and an external product release step.

To ensure that the observed decreases in k_{cat}/K_m and k_{cat} values are due to the increased solvent microviscosity and not interactions with the protein, control experiments were conducted in the presence of a macroviscosogen, PEG 8000, which increases the macroviscosity but not the microviscosity of the solvent.[45] The addition of a macroviscosogen will not perturb rates of small molecule diffusion. The k_{cat} and k_{cat}/K_m values for TpAd in the presence of 5% PEG8000 ($\eta^{rel} = 3$) were found to be unaffected [$k_{cat} = 1.97 \pm 0.10$ s^{-1}; $k_{cat}/K_m = (1.6 \pm 0.4) \times 10^7$ M^{-1} s^{-1}] relative to the values for WT hHint1 determined without the macroviscogen.

In addition, to rule out possible artifactual effects of the viscosogen on the enzyme reaction caused by interactions between the viscosogen and the enzyme or substrate, the effect of viscosity on the hydrolysis of a poor substrate, TrAd (Figure 1; $k_{cat} = 0.27$ s^{-1}; $K_m = 4.1$ μM; $k_{cat}/K_m = 7.0 \times 10^4$ M^{-1} s^{-1}), was determined.[24] Given that a burst phase was not detected by pre-steady-state kinetic analysis for TrAd, a chemical transformation rate, rather than the diffusional rate, can be reasonably assumed to govern the overall reaction rate. As one can see in Figure 3B, the slope of the plot of k_{cat}^0/k_{cat} versus the relative viscosity was found to be 0.08 or close to zero, indicating little or no effect of the viscosogen on the chemical steps of the reaction.

Catalytic Trapping Experiment and Simulation. The pre-steady-state kinetic data suggest that the acylation step for hHint1 is fast and does not limit maximal turnover (Figure 4). To establish whether the deacylation step or possibly a product release step (AMP dissociation) could limit turnover, we performed a catalytic trapping experiment. In this experiment, the enzyme is preequilbrated with the product, AMP, in one syringe of the stopped-flow machine before the reaction is started with the substrate TpAd in the second syringe (Figure 5A). In the absence of AMP, a burst phase followed by a slower linear phase is observed (Figure 5B). These data are best simulated using the two-step kinetic scheme in Figure 5A, where k_1' and k_2' are set to 7.2×10^6 M^{-1} s^{-1} and 0.5 s^{-1}, respectively. The former corresponds to the rate constant for intermediate formation and is close in value to the steady-state k_{cat}/K_m for TpAd (Table 2). The latter corresponds to the net rate constant for deacylation and includes not only the breakdown of the intermediate but also the release of the product AMP and any potential conformational steps. When the enzyme is preequilibrated with 2500 μM AMP, the kinetic transient begins to deviate from the simple biphasic transient observed in the absence of AMP (Figure 5C). A rapid burst of

dx.doi.org/10.1021/bi301616c | *Biochemistry* 2013, 52, 3588−3600

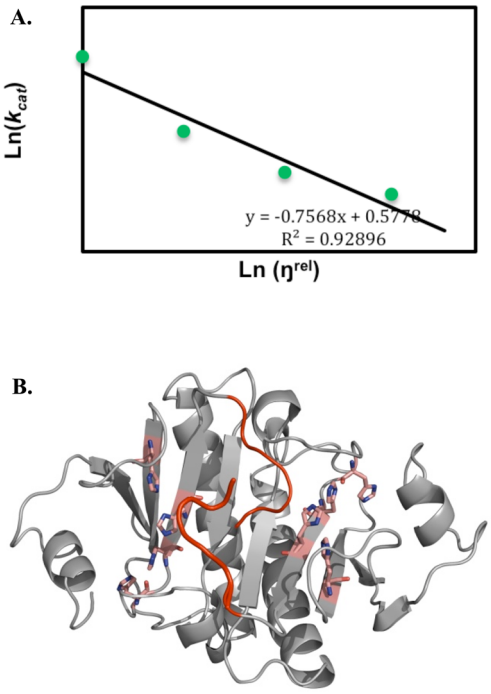

Figure 4. (A) Data from the viscosity experiment were fit to Kramer's model (eq 16), where $\ln(k_{cat})$ is linearly dependent on $\ln(\eta^{rel})$ with a slope of −0.76 (R^2 = 0.93), indicating a strong coupling of product release with the active site conformational change. (B) C-Terminus of the hHint1 homodimer that is proposed to undergo a conformational change coupled to AMP release. The active sites are colored pink, and the C-terminus is colored red.

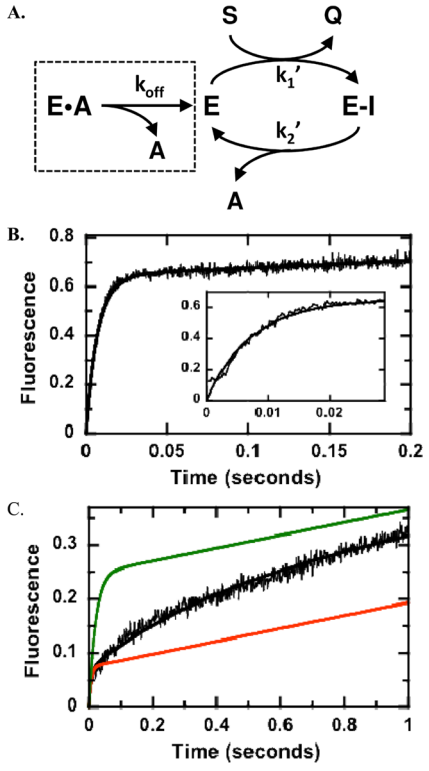

Figure 5. Catalytic trapping of AMP. (A) Kinetic mechanism. Data in the absence and presence of AMP are simulated using DynaFit and a two-step acylation−deacylation mechanism. (B) Kinetic transient in the absence of AMP. Hint1 (5 μM) was mixed with TpAd (20 μM) in the stopped-flow instrument, and the fluorescence changes were simulated using the kinetic scheme in panel A, where k_1' and k_2' are 7.2 μM^{-1} s^{-1} and 0.5 s^{-1}, respectively, and the output for Q is 0.26 V/mM. (C) Kinetic transient in the presence of 2500 mM AMP. Conditions are the same as in panel B except 2500 mM AMP was preequilbrated with the enzyme prior to mixing. The fluorescence changes were simulated using fixed values for k_1' and k_2' from panel B, 0.7 and 1.8 mM E and E·A, an output for Q of 0.1 V/mM, and a k_{off} of 2.7 s^{-1} (black). The data were also simulated using k_{off} values of 50 s^{-1} (green) and 0.5 s^{-1} (red).

fluorescence is followed by a slow exponential phase and a linear phase that corresponds to steady-state product formation. The initial rapid burst has a rate similar to that of the control, albeit with a lower amplitude, suggestive of a small amount of free enzyme in the cuvette prior to the start of the reaction with TpAd. We measured a K_d of 200 μM for AMP to Hint1 in fluorescence titration experiments (Figure S2 of the Supporting Information), indicating that some of the enzyme is likely to exist in an uncomplexed form in the syringe prior to mixing. The slow exponential phase is consistent with rapid exchange of AMP at the active sites, although the dissociation of AMP could be fast. To analyze this kinetic transient, we, therefore, simulated the trapping data with a small amount of free enzyme (0.7 μM) along with a larger amount of the E·A complex (1.8 μM). Using fixed values of k_1 and k_2 from the control simulation lacking product equilibration, a best fit to the kinetic trapping data was obtained using a k_{off} of 2.7 s^{-1} (Figure 5C). Expected kinetic transients assuming that k_{off} is either equal to or 100-fold larger than k_2' are shown for comparison in Figure 5C, demonstrating the capability of sensitively monitoring changes in the AMP release rate. Overall, the catalytic trapping data illustrate that AMP release is not a significant factor controlling the deacylation step and is thus likely to play an only partial role in defining k_{cat}.

pH Dependence of hHint1 Adenylylation. To address the ionization state of residues that are critical for hHint1 adenylylation, the effect of pH on the pre-steady-state kinetics was determined over the pH range of 5.8−9.0 using either AIPA (2.5−20 μM) or TpAd (5−30 μM) as the substrate. For both substrates, the data were best fit with eq 12, according to a mechanism involving three protonic forms, only two (EH and E) of which are active (Scheme 2). The adenylylation rate constants for EH and E were represented as $(k_2)_{lim}$ and $r(k_2)_{lim}$, where r represents the ratio relative to the rate for EH ($0 < r < 1$). The pH versus k_2 profile indicated a dependence of two ionizable groups with pK_a values around 6.6 and 8.0 (6.68 ± 0.09 and 8.03 ± 0.16 for AIPA and 6.56 ± 0.13 and 7.90 ± 0.24 for TpAd). Similar values of $(k_2)_{lim}$ were fit for AIPA (673 ± 50 s^{-1}) and TpAd (634 ± 86 s^{-1}) (Figure 6A). A ratio (r) of k_2 values in two ionization states (E vs EH) of 0.72 ± 0.11 was fit for AIPA, indicating the deprotonated form (E) is 72% active compared to the EH form. In contrast, an r value of 0.16 ± 0.07 (E vs EH) was fit for TpAd, suggesting the E form is only 16% active compared to the EH form. This accounts for the rapid decrease in k_2 in the basic limb of the pH profile for TpAd.

On the other hand, the acid limbs of pH versus $k_2/K^{adenylyl}$ for AIPA and TpAd showed relatively flat curves, indicating the substrates are sticky and the apparent pK_a values are displaced to lower pH values (Figure 6B). Because both curves exhibited a change of only one-half of a log unit in the value of $k_2/K^{adenylyl}$ over a single pH unit, the apparent pK_a values are unlikely to represent the titration of a single ionizable group in the adenylylation reaction.

dx.doi.org/10.1021/bi301616c | *Biochemistry* 2013, 52, 3588−3600

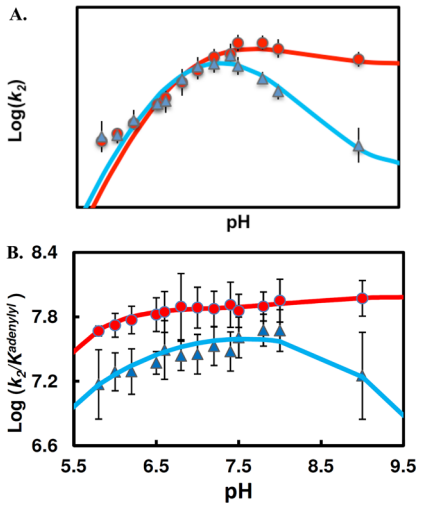

Figure 6. pH dependence of pre-steady-state kinetic parameters of adenylylation of the enzyme by TpAd (▲) and AIPA (●). (A) Plots of adenylylation rate (k_2) vs pH. The data fitting (Scheme 2, eq 12) for the AIPA reaction (red) yielded the following values: pK_1 = 6.68 ± 0.09, pK_2 = 8.03 ± 0.16, r = 0.72 ± 0.11, $(k_2)_{lim}$ = 673 ± 50 s^{-1}. The data fitting for the TpAd reaction (blue) yielded the following values: pK_1 = 6.56 ± 0.13, pK_2 = 7.90 ± 0.24, r = 0.16 ± 0.08, and $(k_2)_{lim}$ = 634 ± 86 s^{-1}. (B) Plots of $k_2/K^{adenylyl}$ vs pH. The pH profiles for the AIPA reaction (red) and the TpAd reaction (blue) were relatively flat, indicating substrates are sticky.

pH Dependence of Steady-State Kinetic Parameters. The dependence of the steady-state substrate hydrolysis on pH was determined with saturating concentrations of AIPA or TpAd (Figure 7). Because the observed steady-state rates for

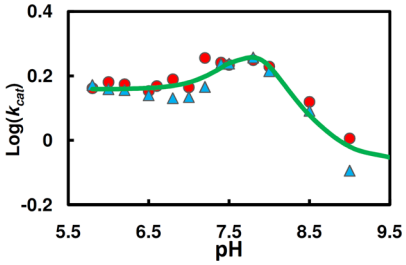

Figure 7. Comparison of the pH [(▲) TpAd and (●) AIPA] dependence of steady-state kinetic parameters (k_{cat}). The pH profile data were fit by eq 13 (Scheme 3), yielding the following values: pK_1 = 7.52 ± 0.18, pK_2 = 8.15 ± 0.10, r = 7.3 ± 2.0, and q = 1.68 ± 0.16. $(k_{cat})_{lim}$ values for the three active forms (AMP-EH_2, AMP-EH, and AMP-E) are 1.44 ± 0.08, 6.28 ± 0.56, and 0.85 ± 0.05 s^{-1}, respectively.

AIPA and TpAd are similar at each pH, the pH versus k_{cat} profile for the hHint1-catalyzed reaction was found to be best fit by a minimal two-pK_a model with three active forms (Scheme 3), yielding a pK_{a1} of 7.52 ± 0.18 and a pK_{a2} of 8.15 ± 0.10, and k_{cat} values for the three states, EH_2, EH, and E, of 1.44 ± 0.08, 6.28 ± 0.56, and 0.85 ± 0.05 s^{-1}, respectively. Because the hydrolysis of adenylylated Hint1 and product release are partially rate-limiting in the steady state, the pH profile presumably reflects the overall effects of pH on both steps.[46]

Determination of the Uncatalyzed Rate of TpAd and AIPA Hydrolysis. The hydrolysis of AIPA, and TpAd, as monitored by the disappearance of the peak at 5.88 ppm, proceeded to completion with first-order kinetics. The results

Scheme 3

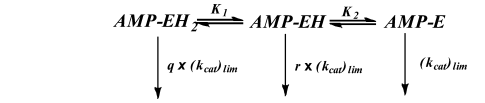

$$(k_{cat})_{obs} = \frac{q\times(k_{cat})_{lim}}{1+\frac{K_1}{[H^+]}+\frac{K_1K_2}{[H^+]^2}} + \frac{r\times(k_{cat})_{lim}}{\frac{[H^+]}{K_1}+1+\frac{K_2}{[H^+]}} + \frac{(k_{cat})_{lim}}{1+\frac{[H^+]^2}{K_1K_2}+\frac{[H^+]}{K_2}}$$

$$\log(k_{cat})_{obs} = \log\left(\frac{q\times(k_{cat})_{lim}\times10^{(pK_1-pH)} + r\times(k_{cat})_{lim} + (k_2)_{lim}\times10^{(pH-pK_2)}}{10^{(pH-pKa_2)}+1+10^{(pKa_1-pH)}}\right) \quad (13)$$

yielded a linear Arrhenius plot with a k_{25} of 1.1 × 10^{-6} s^{-1} at 25 °C and a $\Delta H^{\ddagger}$ of 20.1 kcal/mol at pH 6.8 for AIPA and a k_{25} of 2.0 × 10^{-8} s^{-1} at 25 °C and a $\Delta H^{\ddagger}$ of 16.9 kcal/mol at pH 6.8 for TpAd (Figure 8). For AIPA, the rate of hydrolysis increased

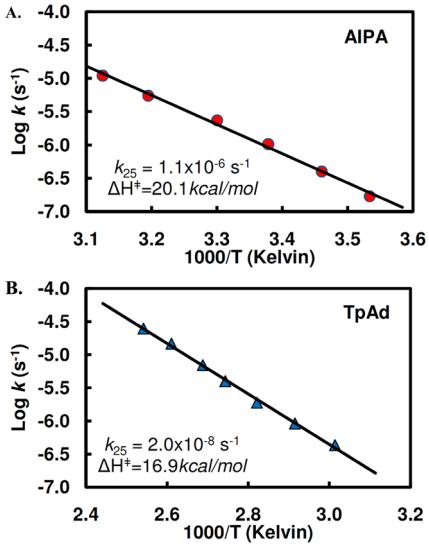

Figure 8. Arrhenius plots for hydrolysis of AIPA (A) and TpAd (B) at 25 °C and pH 6.8.

monotonically with an increase in pH, by a factor of ~3 in the region between pH 4.8 (0.1 M potassium acetate) and pH 8.4 (0.1 M potassium borate), while for TpAd, the rate decreased by a factor of 3 over the same pH range.

pH Dependence of the Chemical Shifts of Active Site hHint1 Histidines. To assist in understanding the pH dependence of the pre-steady-state and steady-state kinetics of hHint1, the effect on the chemical shifts of the active site histidines was determined. Representative 1D proton TOCSY spectra for hHint1 in D_2O are shown in Figure S4 of the Supporting Information. Of the six well-resolved histidine C-2 proton resonances in the region of 7.5−9 ppm, one titratable signal was identified. By comparison with the spectra of the His112Gly and His112Ala mutants at pH 7.5, this side chain resonance could be assigned to His112. Fitting with the modified Henderson−Hasselbalch equation (eq 15) of the pH versus C-2 chemical shift (δ) plot yielded a pK_a value for His112 of 6.50 ± 0.06.

■ DISCUSSION

Interest in Hint proteins has grown since it was discovered that they are involved in a variety of biological processes across all kingdoms of life.[47] Hints have been shown to be highly efficient nucleoside phosphoramidases and acyl-AMP hydrolases.[37]

dx.doi.org/10.1021/bi301616c | Biochemistry 2013, 52, 3588−3600

Nevertheless, the biological relevance of the catalytic activity of Hints has remained obscure. In three cases, Hint catalysis has been clearly shown to be essential. Brenner and co-workers have demonstrated that yeast deficient in catalyically active Hint1 homologue, HNT1, is unable to grow on galactose at elevated temperatures.[48] In addition, they found that HNT1 was a regulator of the TFIIH kinase subcomplex of the transcription complex, TFIIH, and the Cdk7 ortholog, Kin28.[48] Our laboratory has demonstrated that *E. coli* also encodes only one Hint protein, ecHinT. We have also shown that catalytically active ecHinT is necessary for the growth of *E. coli* under high-salt conditions.[23] In addition, the ability of *E. coli* to grow on alanine was shown to depend on the catalytic regulation of D-amino acid dehydrogenase activity by ecHinT.[30] In addition, recently, the first example association of hHint1 with a human phenotype has been discovered by the demonstration that inherited peripheral neuropathy is caused by the loss of hHint1 function due to at least eight different mutations.[1] Mutations of two of these residues are known to affect catalytic activity (His51) or result in the loss of catalytic activity (His112).[1,49]

Detailed catalytic and kinetic mechanistic studies have been conducted with only the DcpS subfamily of the HIT superfamily, while catalytic studies have been pursued with GalT, Fhit, and Hint1. Preliminary studies of the catalytic mechanism of Hints have revealed that (1) of the four conserved active site histidines, one is essential for catalytic activity,[26] (2) the reaction proceeds through an active site His–AMP intermediate,[26] and (3) the pre-steady-state kinetics are characterized by a burst phase followed by a linear rate.[50] To begin to elucidate the kinetic mechanism of Hint1s, we chose to characterize the kinetic mechanism of hHint1.

The transient burst followed by a linear phase observed during earlier stopped-flow experiments for ecHinT was also observed for hHint1.[50] This observation is consistent with our hypothesis that hHint1 proceeds by rapid formation of the AMP–Hint intermediate, followed by at least partial rate-limiting hydrolysis of the intermediate. The rate of the burst phase was found to be substrate-dependent (k_2 = 443 and 203 s^{-1} for AIPA and TpAd, respectively), whereas nearly identical values for the overall turnover numbers were observed for both substrates. Moreover, the different burst rates for TpAd and AIPA and the inability to observe at least one additional exponential phase suggest that if a conformational change does occur upon substrate binding, it is quite rapid and therefore not kinetically significant. In addition, the transient burst was found to correspond to 77% of the hHint1 monomer concentration. Although the substrate specificity of hHint1 has been shown to be dependent on interactions contributed by the C-terminus of each monomer to the active site of the adjacent monomer,[51] the observation of a burst corresponding to nearly 80% of the hHint1 monomer concentration indicates that the two active sites of hHint1 independently catalyze substrate hydrolysis. The hyperbolic, rather than sigmoidal, relationship of the steady-state rate versus substrate concentration plot further confirmed that kinetically significant cooperative interactions do not exist between the two active sites of hHint. In contrast, the active sites of homodimeric DcpS exhibited negative cooperativity.[52]

Compared to that of TpAd, burst kinetics was not observed for the less efficient substrate, TrAd, and the linear rate corresponded to the steady-state k_{cat} value. In addition, the k_{cat} for TrAd (k_{cat} = 0.27 s^{-1}) was found to be 7.7-fold lower than the k_{cat} for TpAd.[24] Thus, the k_{cat} for the poor substrate, TrAd, is likely due to rate-limiting active site adenylylation, because the rate of enzyme–AMP intermediate hydrolysis and subsequent AMP dissociation would be independent of the alkyl amine leaving group. The rate of hHint1 adenylylation by TpAd is thus shown to be 17000-fold greater than the rate observed for TrAd. Consequently, the rate of the first step of the kinetic mechanism is profoundly affected by the alkyl amine of the nucleoside phosphoramidate substrate.

Because enzyme adenylylation by TpAd is rapid and not rate-limiting, either intermediate hydrolysis, product release, or a combination of these two steps should govern the overall substrate turnover for hHint1. Since the rates of kinetically significant steps can be dependent on the nature of the solvent, the effect of solvent viscosity on enzyme catalysis has been extensively evaluated. For example, Townsend and co-workers have elegantly applied a series of solvent viscosity studies to elucidate the rate-limiting steps of carbapenam synthetase and β-lactam synthetase.[53] Consequently, we chose to characterize the rate-limiting steps of hHint1 with a series of solvent effect studies. Steady-state kinetic studies conducted with increasing concentrations of a microviscogen, sucrose, revealed that the second-order rate constant (k_{cat}/K_m) was significantly affected, while the overall reaction rate (k_{cat}) was only modestly affected. By plotting the relative k_{cat}/K_m values versus relative viscosity, we can determine the dependence of all the reaction processes on diffusional control preceding and including the first irreversible step.[39,54] The significant sensitivity of the k_{cat}/K_m of TpAd to viscosity (slope of 0.9) suggests that the steps preceding the first irreversible step, hHint1 adenylylation, are under diffusional control. Likewise, the viscosity dependence of k_{cat} provides an estimate of the extent to which the turnover number is limited by product diffusional release. The observed k_{cat} for TpAd was found to be moderately sensitive to solvent viscosity (a slope of ~0.6), implying that product release accounts for approximately half of the overall rate (k_{cat}). On the basis of these results, we propose that hHint1 catalysis proceeds minimally through a four-step kinetic mechanism (Scheme 1).

To further characterize the release of AMP by hHint1, catalytic trapping experiments and fluorescence titration experiments were conducted. The burst amplitude was indeed shown to be dependent on the AMP concentration, which is consistent with AMP release being at least partially rate-limiting. Simulation of catalytic trapping data showed the true dissociation rate of AMP (k_{off}) may not be significant in determining the overall k_{cat}. Examination of the effects of viscosity on k_{cat} using Kramer's model (eq 16) indicated that the association of a conformational change and product release contributed to the viscosity effect (Figure 4).

$$k_{cat} = A\eta^{-\delta} e^{E_a/kT} \quad (16)$$

Nevertheless, hHint1 has a very low affinity for AMP. Because both the K_i determined by the catalytic trapping studies (Figure S3 of the Supporting Information) and the K_d determined by fluorescence titration experiments for AMP (Figure S2 of the Supporting Information) were found to be approximately 200 μM, the association rate constant for AMP is quite low.

Given the results of the steady-state and pre-steady-state kinetics and the viscosity experiments, the rate constants for the proposed minimal kinetic mechanism for hHint1 can be assembled on the basis of Scheme 1. First, on the basis of the slopes of the plot of $(k_{cat}/K_m)^0/(k_{cat}/K_m)$ versus relative viscosity for AIPA and TpAd (Figure 3A) and the burst rates for each substrate (k_2), eq 9 can be employed to calculate values

Scheme 4. Proposed Kinetic Mechanism of hHint1 with Substrates AIPA and TpAd

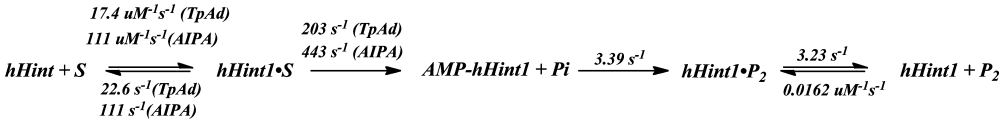

of 111 and 22.6 s^{-1} for the rate of substrate dissociation (k_{-1}) for AIPA and TpAd, respectively (Scheme 4). Knowing the values of k_2 and k_{-1}, we can then calculate the values of k_1 from eq 4 for $K^{adenylyl}$, yielding second-order rate constants of 111 and 17.4 μM^{-1} s^{-1} for AIPA and TpAd, respectively. Next, employing eq 11 and the slope and intercept of the plot of $1/k_{cat}$ versus the relative viscosity for TpAd (Figure 3C), values of 3.23 and 3.38 s^{-1} could be determined for k_3 and k_{-4}, respectively. Lastly, given a K_d for AMP of 200 μM, and the value of k_{-4}, a value of 0.0162 μM^{-1} s^{-1} could be calculated for the association rate constant for AMP.

With the derived rate constants in hand, k_{cat} values of 1.63 ± 0.01 and 1.65 ± 0.03 s^{-1} for TpAd and AIPA, respectively, and K_m values of 0.131 ± 0.004 and 0.039 ± 0.005 μM for TpAd and AIPA, respectively, were derived. The simulated k_{cat} and K_m values correspond closely to the experimental values (Table 2) for k_{cat} values of 1.98 ± 0.02 and 2.0 ± 0.1 s^{-1} for TpAd and AIPA, respectively, and K_m values of 0.13 ± 0.02 and 0.040 ± 0.002 μM for TpAd and AIPA, respectively, thus providing support for the proposed kinetic mechanism. In addition, although the dissociation of AMP from the enzyme was found by kinetic viscosity studies to be coupled to hHint1 conformational changes, the rates of these steps cannot be observed and therefore appear not to be kinetically significant.

We hypothesize that the binding of AMP to hHint1, as well as AMP release, is potentially coupled to conformational changes induced by the flexible C-terminus. Deletion of the C-terminus of hHint1 results in a 200−400-fold decrease in the rate of hHint1 adenylylation and a 100−200-fold decrease in the overall rate. Future studies, delineating the role of the dynamics of the C-terminus in hHint1 product release, should help address this hypothesis.

The kinetic mechanism of hHint1 outlined has been established for pH 7.0. The active site of hHint1, however, is composed of four histidines, including a nucleophilic histidine (His112), which is adenylylated by both AIPA and TpAd. As expected, pH versus rate studies for enzyme adenylylation exhibited a strong pH dependence with observable pK_a values of 6.68 and 8.03 for AIPA and 6.51 and 7.90 for TpAd. In both cases, the first pK_a was found to correspond to the pK_a of 6.5 determined by NMR titration of His112. We noticed that the pH versus k_2 profile for TpAd differs from that for AIPA at the basic limb, indicating that the deprotonated form (E) is less able to catalyze the TpAd reaction (r = 0.16) than AIPA hydrolysis (r = 0.72) (Scheme 2 and Figure 6A). This discrepancy can be explained by the dependence of the rate of adenylylation on an ionizable group with a pK_a of approximately 8. Deprotonation of this group at pH >8 would result in a decrease in the rate of adenylylation for TpAd, with little effect on the adenylation rate for AIPA. We propose that H114 could be this ionizable group and act as a proton donor in Hint1 adenylylation (Figure 1A) by facilitating protonation of either the tryptamine or indole proprionic acid leaving groups during hydrolysis of TpAd or AIPA, respectively.

Two pK_a values of 7.52 and 8.15 were observed for the pH versus k_{cat} profile. Because both hydrolysis of the adenylylated enzyme and product release are partially rate-limiting, neither pK_a should correspond to free His112. The pK_a of adenylylated imidazole has been shown to be 5.4, significantly reducing the efficiency of P−N bond cleavage at physiological pH.[55] It is more likely that the second pK_a corresponds to the protonated imidazole for adenylylated His112, while the first pK_a corresponds to an active site acid, possibly His114.

While the natural substrates for hHint1 are presently unknown, the enzyme efficiently hydrolyzes both acyl-AMP and nucleoside phosphoramidates with k_{cat}/K_m values at or near the diffusion control for AIPA and TpAd. The work of Wolfenden and co-workers has demonstrated that enzymes can accelerate the rate of a reaction by factors ranging from 10^5- to 10^{17}-fold.[56,57] To assess the rate enhancements produced by hHint1 for substrate hydrolysis, we determined the rate constants for the uncatalyzed hydrolysis of the anhydride AIPA (k_{25} = 1.1 × 10^{-6} s^{-1}) and the phosphoric amide TpAd (k_{25} = 2.0 × 10^{-8} s^{-1}). These values are considerably smaller than the rate constants that have been reported for the uncatalyzed hydrolysis of unsubstituted acetyl phosphate (k_{39} = 1.9 × 10^{-3} s^{-1}) and phosphoric acid amide (k_{37} = 1.2 × 10^{-4} s^{-1}),[58,59] presumably reflecting the accessibility of ionic species of these unsubstituted molecules that are more reactive than AIPA or TpAd. Considering that AIPA and TpAd are unnatural substrates, it is of interest that hHint1 accelerates AIPA hydrolysis by a factor of 10^6 and TpAd hydrolysis by a factor of 10^8, with enzyme efficiencies (k_{cat}/K_m) rivaling those of well-known enzymes, such as cytidine deaminase and carboxypeptidase B.[60] Thus, although AIPA and TpAd are unnatural substrates, hHint1 seems to be highly evolved to cleave both substrates. While the recent discovery that Hints and in particular forms of Hint1 are able to hydrolyze AARS-generated amino acyl-AMPs may ultimately explain their preference for AIPA, the rationale for their phosphoramidase activity remains to be discovered.

■ ASSOCIATED CONTENT

Supporting Information

Pre-steady-state kinetics of formation of the adenylated enzyme intermediate (Figure S1), dissociation constants (K_d) of AMP determined by fluorescence titration of hHint1 (Figure S2), determination of K_i values for AMP in catalytic trapping experiments (Figure S3), and NMR analysis of histidine pK_a values in hHint1 (Figure S4). This material is available free of charge via the Internet at http://pubs.acs.org.

■ AUTHOR INFORMATION

Corresponding Author

*Department of Medicinal Chemistry, University of Minnesota, 8-174 Weaver Densford Hall, 308 Harvard St. S.E., Minneapolis, MN 55455. E-mail: wagne003@umn.edu. Fax: (612) 624-0139. Telephone: (612) 624-2614.

Funding

Partial funding of this study by the University of Minnesota Endowment and National Institutes of Health Grant GM-18325 (R.W.) is gratefully acknowledged.

Notes

The authors declare no competing financial interest.

■ ABBREVIATIONS

Hint, histidine triad nucleotide binding protein; hHint1, human histidine nucleotide binding protein 1; AIPA, adenosine 5′-indole-3-propionic adenylate; GalT, galactose-1-phosphate uridyl transferase; HIT, histidine triad; PDB, Protein Data Bank; TpAd, tryptamine adenosine phophoramidate monoester; TrAd, 2(*R*)-adenosyl-5′-(phophorylamino)-3-(3-indolyl)propionic acid methyl ester; Fhit, fragile histidine triad; WT, wild type.

■ REFERENCES

(1) Zimon, M., Baets, J., Almeida-Souza, L., De Vriendt, E., Nikodinovic, J., Parman, Y., Battaloglu, E., Matur, Z., Guergueltcheva, V., Tournev, I., Auer-Grumbach, M., De Rijk, P., Petersen, B.-S., Muller, T., Fransen, E., Van Damme, P., Loscher, W. N., Barisic, N., Mitrovic, Z., Previtali, S. C., Topaloglu, H., Bernert, G., Beleza-Meireles, A., Todorovic, S., Savic-Pavicevic, D., Ishpekova, B., Lechner, S., Peeters, K., Ooms, T., Hahn, A. F., Zuchner, S., Timmerman, V., Van Dijck, P., Rasic, V. M., Janecke, A. R., De Jonghe, P., and Jordanova, A. (2012) Loss-of-function mutations in HINT1 cause axonal neuropathy with neuromyotonia. *Nat. Genet. 44*, 1080−1083.

(2) Brenner, C., Garrison, P., Gilmour, J., Peisach, D., Ringe, D., Petsko, G. A., and Lowenstein, J. M. (1997) Crystal structures of HINT demonstrate that histidine triad proteins are GalT-related nucleotide-binding proteins. *Nat. Struct. Biol. 4*, 231−238.

(3) Mozier, N. M., Walsh, M. P., and Pearson, J. D. (1991) Characterization of a novel zinc binding site of protein kinase C inhibitor-1. *FEBS Lett. 279*, 14−18.

(4) Lima, C. D., Klein, M. G., Weinstein, I. B., and Hendrickson, W. A. (1996) Three-dimensional structure of human protein kinase C interacting protein 1, a member of the HIT family of proteins. *Proc. Natl. Acad. Sci. U.S.A. 93*, 5357−5362.

(5) Rodriguez-Munoz, M., de la Torre-Madrid, E., Sanchez-Blazquez, P., Wang, J. B., and Garzon, J. (2008) NMDAR-nNOS generated zinc recruits PKCγ to the HINT1-RGS17 complex bound to the C terminus of Mu-opioid receptors. *Cell. Signalling 20*, 1855−1864.

(6) Ajit, S. K., Ramineni, S., Edris, W., Hunt, R. A., Hum, W. T., Hepler, J. R., and Young, K. H. (2007) RGSZ1 interacts with protein kinase C interacting protein PKCI-1 and modulates mu opioid receptor signaling. *Cell. Signalling 19*, 723−730.

(7) Weiske, J., and Huber, O. (2006) The histidine triad protein Hint1 triggers apoptosis independent of its enzymatic activity. *J. Biol. Chem. 281*, 27356−27366.

(8) Korsisaari, N., and Makela, T. P. (2000) Interactions of Cdk7 and Kin28 with Hint/PKCI-1 and Hnt1 histidine triad proteins. *J. Biol. Chem. 275*, 34837−34840.

(9) Razin, E., Zhang, Z. C., Nechushtan, H., Frenkel, S., Lee, Y. N., Arudchandran, R., and Rivera, J. (1999) Suppression of microphthalmia transcriptional activity by its association with protein kinase C-interacting protein 1 in mast cells. *J. Biol. Chem. 274*, 34272−34276.

(10) Lee, Y. N., Nechushtan, H., Figov, N., and Razin, E. (2004) The function of lysyl-tRNA synthetase and Ap4A as signaling regulators of MITF activity in FcεRI-activated mast cells. *Immunity 20*, 145−151.

(11) Lee, Y. N., and Razin, E. (2005) Nonconventional involvement of LysRS in the molecular mechanism of USF2 transcriptional activity in FcεRI-activated mast cells. *Mol. Cell. Biol. 25*, 8904−8912.

(12) Cen, B., Li, H., and Weinstein, I. B. (2009) Histidine triad nucleotide-binding protein 1 up-regulates cellular levels of p27KIP1 by targeting ScfSKP2 ubiquitin ligase and Src. *J. Biol. Chem. 284*, 5265−5276.

(13) Cen, B., Deguchi, A., and Weinstein, I. B. (2008) Activation of protein kinase G increases the expression of p21CIP1, p27KIP1, and histidine triad protein 1 through Sp1. *Cancer Res. 68*, 5355−5362.

(14) Li, H., Zhang, Y., Su, T., Santella, R. M., and Weinstein, I. B. (2006) Hint1 is a haplo-insufficient tumor suppressor in mice. *Oncogene 25*, 713−721.

(15) Weiske, J., and Huber, O. (2006) The histidine triad protein Hint1 triggers apoptosis independent of its enzymatic activity. *J. Biol. Chem. 281*, 27356−27366.

(16) Korsisaari, N., Rossi, D. J., Luukko, K., Huebner, K., Henkemeyer, M., and Makela, T. P. (2003) The histidine triad protein Hint is not required for murine development or Cdk7 function. *Mol. Cell. Biol. 23*, 3929−3935.

(17) Barbier, E., Zapata, A., Oh, E., Liu, Q., Zhu, F., Undie, A., Shippenberg, T., and Wang, J. B. (2007) Supersensitivity to amphetamine in protein kinase-C interacting protein/HINT1 knockout mice. *Neuropsychopharmacology 32*, 1774−1782.

(18) Chen, Q., Wang, X., O'Neill, F. A., Walsh, D., Kendler, K. S., and Chen, X. N. (2008) Is the histidine triad nucleotide-binding protein 1 (HINT1) gene a candidate for schizophrenia. *Schizophr. Res. 106*, 200−207.

(19) Martin, J., Romanque, P., Maurhofer, O., Schmitter, K., Hora, C., Ferrand, G., and Dufour, J. F. (2011) Ablation of the Tumor Suppressor Histidine Triad Nucleotide Binding Protein 1 is Protective Against Hepatic Ischemia/Reperfusion Injury. *Hepatology 53*, 243−252.

(20) Pace, H. C., and Brenner, C. (2003) Feminizing chicks: A model for avian sex determination based on titration of Hint enzyme activity and the predicted structure of an Asw-Hint heterodimer. *Genome Biol. 4*, R18.

(21) Parks, K. P., Seidle, H., Wright, N., Sperry, J. B., Bieganowski, P., Howitz, K., Wright, D. L., and Brenner, C. (2004) Altered specificity of Hint-W123Q supports a role for Hint inhibition by ASW in avian sex determination. *Physiol. Genomics 20*, 12−14.

(22) Krakowiak, A., Pace, H. C., Blackburn, G. M., Adams, M., Mekhalfia, A., Kaczmarek, R., Baraniak, J., Stec, W. J., and Brenner, C. (2004) Biochemical, crystallographic, and mutagenic characterization of hint, the AMP-lysine hydrolase, with novel substrates and inhibitors. *J. Biol. Chem. 279*, 18711−18716.

(23) Chou, T. F., Bieganowski, P., Shilinski, K., Cheng, J., Brenner, C., and Wagner, C. R. (2005) ^{31}P NMR and genetic analysis establish hinT as the only *Escherichia coli* purine nucleoside phosphoramidase and as essential for growth under high salt conditions. *J. Biol. Chem. 280*, 15356−15361.

(24) Chou, T. F., Baraniak, J., Kaczmarek, R., Zhou, X., Cheng, J., Ghosh, B., and Wagner, C. R. (2007) Phosphoramidate pronucleotides: A comparison of the phosphoramidase substrate specificity of human and *Escherichia coli* histidine triad nucleotide binding proteins. *Mol. Pharmaceutics 4*, 208−217.

(25) Wagner, C. R., Iyer, V. V., and McIntee, E. J. (2000) Pronucleotides: Toward the in vivo delivery of antiviral and anticancer nucleotides. *Med. Res. Rev. 20*, 417−451.

(26) Chou, T. F., and Wagner, C. R. (2007) Lysyl-tRNA synthetase-generated lysyl-adenylate is a substrate for histidine triad nucleotide binding proteins. *J. Biol. Chem. 282*, 4719−4727.

(27) Wang, J., Fang, P., Schimmel, P., and Guo, M. (2012) Side chain independent recognition of aminoacyl adenylates by the Hint1 transcription suppressor. *J. Phys. Chem. B 116*, 6798−6805.

(28) Ozga, M., Dolot, R., Janicka, M., Kaczmarek, R., and Krakowiak, A. (2010) Histidine triad nucleotide-binding protein 1 (Hint-1) phosphoramidase transforms nucleoside 5′-O-phosphorothioates to nucleoside 5′-phosphates. *J. Biol. Chem. 285*, 40809−40818.

(29) Bieganowski, P., Garrison, P. N., Hodawadekar, S. C., Faye, G., Barnes, L. D., and Brenner, C. (2002) Adenosine monophosphoramidase activity of Hint and Hnt1 supports function of Kin28, Ccl1, and Tfb3. *J. Biol. Chem. 277*, 10852−10860.

(30) Bardaweel, S., Ghosh, B., Chou, T. F., Sadowsky, M. J., and Wagner, C. R. (2011) *E. coli* histidine triad nucleotide binding protein 1 (ecHinT) is a catalytic regulator of D-alanine dehydrogenase (DadA) activity in vivo. *PLoS One 6*, e20897.

(31) Geeganage, S., and Frey, P. A. (1998) Transient kinetics of formation and reaction of the uridylyl-enzyme form of galactose-1-P

uridylyltransferase and its Q168R-variant: Insight into the molecular basis of galactosemia. *Biochemistry 37*, 14500−14507.
(32) Wedekind, J. E., Frey, P. A., and Rayment, I. (1996) The structure of nucleotidylated histidine-166 of galactose-1-phosphate uridylyltransferase provides insight into phosphoryl group transfer. *Biochemistry 35*, 11560−11569.
(33) Abend, A., Garrison, P. N., Barnes, L. D., and Frey, P. A. (1999) Stereochemical retention of the configuration in the action of Fhit on phosphorus-chiral substrates. *Biochemistry 38*, 3668−3676.
(34) Huang, K., Arabshahi, A., and Frey, P. A. (2005) pH-dependence in the hydrolytic action of the human fragile histidine triad. *Eur. J. Org. Chem.*, 5198−5206.
(35) Huang, K., Arabshahi, A., Wei, Y., and Frey, P. A. (2004) The mechanism of action of the fragile histidine triad, Fhit: Isolation of a covalent adenylyl enzyme and chemical rescue of H96G-Fhit. *Biochemistry 43*, 7637−7642.
(36) Brenner, C. (2002) Hint, Fhit, and GalT: Function, structure, evolution, and mechanism of three branches of the histidine triad superfamily of nucleotide hydrolases and transferases. *Biochemistry 41*, 9003−9014.
(37) Chou, T. F., Tikh, I. B., Horta, B. A., Ghosh, B., De Alencastro, R. B., and Wagner, C. R. (2007) Engineered monomeric human histidine triad nucleotide-binding protein 1 hydrolyzes fluorogenic acyl-adenylate and lysyl-tRNA synthetase-generated lysyl-adenylate. *J. Biol. Chem. 282*, 15137−15147.
(38) Bradford, M. M. (1976) A rapid and sensitive method for the quantitation of microgram quantities of protein utilizing the principle of protein-dye binding. *Anal. Biochem. 72*, 248−254.
(39) Brouwer, A. C., and Kirsch, J. F. (1982) Investigation of diffusion-limited rates of chymotrypsin reactions by viscosity variation. *Biochemistry 21*, 1302−1307.
(40) Markley, J. L., Finkenstadt, W. R., Dugas, H., Leduc, P., and Drapeau, G. R. (1975) Proton magnetic resonance titration curves of the three histidine residues of staphylococcal protease. *Biochemistry 14*, 998−1005.
(41) Wolfenden, R., Ridgway, C., and Young, G. (1998) Spontaneous hydrolysis of ionized phosphate monoesters and diesters and the proficiencies of phosphatases and phosphodiesterases as catalysts. *J. Am. Chem. Soc. 120*, 833−834.
(42) Chou, T.-F., Baraniak, J., Kaczmarek, R., Zhou, X., Cheng, J., Ghosh, B., and Wagner, C. R. (2007) Phosphoramidate Pronucleotides: A Comparison of the Phosphoramidase Substrate Specificity of Human and E. coli Histidine Triad Nucleotide Binding Proteins (Hint1). *Mol. Pharmaceutics 4*, 208−217.
(43) Bardaweel, S., Pace, J., Chou, T. F., Cody, V., and Wagner, C. R. (2010) Probing the Impact of the EchinT C-terminal Domain on Structure and Catalysis. *J. Mol. Biol. 404*, 672−638.
(44) Johnson, K. A. (1986) Rapid kinetic analysis of mechanochemical adenosinetriphosphatases. *Methods Enzymol. 134*, 677−705.
(45) Blacklow, S. C., Raines, R. T., Lim, W. A., Zamore, P. D., and Knowles, J. R. (1988) Triosephosphate isomerase catalysis is diffusion controlled. Appendix: Analysis of triose phosphate equilibria in aqueous solution by ^{31}P NMR. *Biochemistry 27*, 1158−1167.
(46) Schimerlik, M. I., and Cleland, W. W. (1977) pH variation of the kinetic parameters and the catalytic mechanism of malic enzyme. *Biochemistry 16*, 576−583.
(47) Brenner, C., Bieganowski, P., Pace, H. C., and Huebner, K. (1999) The histidine triad superfamily of nucleotide-binding proteins. *J. Cell. Physiol. 181*, 179−187.
(48) Bieganowski, P., Garrison, P. N., Hodawadekar, S. C., Faye, G., Barnes, L. D., and Brenner, C. (2002) Adenosine monophosphoramidase activity of Hint and Hnt1 supports function of Kin28, Ccl1, and Tfb3. *J. Biol. Chem. 277*, 10852−10860.
(49) Chou, T.-F., and Wagner, C. R. (2007) Lysyl-tRNA synthetase-generated lysyl-adenylate is a substrate for histidine triad nucleotide binding proteins. *J. Biol. Chem. 282*, 4719−4727.
(50) Bardaweel, S., Pace, J., Chou, T. F., Cody, V., and Wagner, C. R. (2010) Probing the impact of the echinT C-terminal domain on structure and catalysis. *J. Mol. Biol. 404*, 627−638.
(51) Chou, T. F., Sham, Y. Y., and Wagner, C. R. (2007) Impact of the C-terminal loop of histidine triad nucleotide binding protein1 (Hint1) on substrate specificity. *Biochemistry 46*, 13074−13079.
(52) Liu, S. W., Rajagopal, V., Patel, S. S., and Kiledjian, M. (2008) Mechanistic and kinetic analysis of the DcpS scavenger decapping enzyme. *J. Biol. Chem. 283*, 16427−16436.
(53) Raber, M. L., Arnett, S. O., and Townsend, C. A. (2009) A conserved tyrosyl-glutamyl catalytic dyad in evolutionarily linked enzymes: Carbapenam synthetase and β-lactam synthetase. *Biochemistry 48*, 4959−4971.
(54) Hardy, L. W., and Kirsch, J. F. (1984) Diffusion-limited component of reactions catalyzed by *Bacillus cereus* β-lactamase I. *Biochemistry 23*, 1275−1282.
(55) Weber, A. L., and Orgel, L. E. (1978) Amino acid activation with adenosine 5′-phosphorimidazolide. *J. Mol. Evol. 11*, 9−16.
(56) Wolfenden, R. (2011) Benchmark reaction rates, the stability of biological molecules in water, and the evolution of catalytic power in enzymes. *Annu. Rev. Biochem. 80*, 645−667.
(57) Edwards, D. R., Lohman, D. C., and Wolfenden, R. (2012) Catalytic Proficiency: The Extreme Case of S-O Cleaving Sulfatases. *J. Am. Chem. Soc. 134*, 525−531.
(58) Koshland, D. E. (1952) Effect of catalysts on the hydrolysis of acetyl phosphate. Nucleophilic displacement mechanisms in enzymatic reactions. *J. Am. Chem. Soc. 74*, 2286−2292.
(59) Chanley, J. D., and Feageson, E. (1963) A study of the hydrolysis of phosphoramides. II. Solvolysis of phosphoramidic acid. *J. Am. Chem. Soc. 85*, 1181−1190.
(60) Wolfenden, R., and Snider, M. J. (2001) The depth of chemical time and the power of enzymes as catalysts. *Acc. Chem. Res. 34*, 938−945.